Z. Phys. Chem. **225** (2011) 939–956 / **DOI** 10.1524/zpch.2011.0137

Relaxation Dynamics of Electronically Excited C_{60}^- in o-Dichlorobenzene and Tetrahydrofuran Solution

By Helge Brands[1], Oli T. Ehrler[2], Manfred Kappes[3,4,5], and Andreas-Neil Unterreiner[3,4,*]

[1] Paul Scherrer Institute, WBGB/013, 5232 Villigen PSI, Switzerland
[2] Carl Zeiss SMT GmbH/Laser Optics GmbH, Carl-Zeiss-Str. 22, 73447 Oberkochen, Germany
[3] Karlsruhe Institute of Technology (KIT), Institute for Physical Chemistry, 76049 Karlsruhe, Germany
[4] Karlsruhe Institute of Technology (KIT), Center for Functional Nanostructures, 76049 Karlsruhe, Germany
[5] Karlsruhe Institute of Technology (KIT), Institute for Nanotechnology, 76049 Karlsruhe, Germany

Dedicated to Prof. Horst Hippler on the occasion of his 65th birthday

(Received June 30, 2011; accepted in revised form July 30, 2011)

Charged C_{60} / Fullerenes / Excited State Lifetime / Solvent Dependence / Transient Anisotropy / Pseudorotation

The ultrafast response of singly negatively charged C_{60} fullerene in solution has been investigated by femtosecond pump-probe absorption spectroscopy and transient anisotropy in the visible and near-infrared region. Pump excitation within the near-infrared band demonstrates that this spectral feature can be described as a vibrational progression associated with a single electronic transition. Relaxation of the first electronically excited state occurs primarily by internal conversion with a time constant of 3 ps, slightly depending on the solvents, tetrahydrofuran or o-dichlorobenzene, and also on the excitation wavelength. An excitation of the second electronically excited state around 530 nm leads to an ultrafast internal conversion to the first excited state with a pulse-limited time constant of less than 100 fs. As a minor channel, stimulated emission in the spectral regime of 1150–1300 nm was observed from the first electronically excited state both after near-infrared and visible excitation. After internal conversion to the electronic ground state, C_{60}^- dissipates its excess internal energy into the solvent on a longer timescale of 40–70 ps. The transient anisotropy associated with directly populating the first excited state reveals an ultrafast component decaying within 100 fs, which is attributed to ultrafast vibrational motions, conceivably arising from excited state pseudorotation.

1. Introduction

The elucidation of photoinduced energy and electron transfer steps is one of the main issues in understanding the underlying mechanisms of light-harvesting systems. This is also relevant for the design of new electronic devices, solar cell systems or supramolecular aggregates. Various model systems have been proposed and intensively investi-

* Corresponding author. E-mail: andreas.unterreiner@kit.edu

gated. Among them are the icosahedral symmetry C_{60} cage (= buckminsterfullerene) as well as larger fullerene homologues. Especially its capability as a good electron acceptor has made $C_{60}(I_h)$ an interesting candidate for investigations of photophysics in various environments, in which strong vibrational coupling significantly influences electronic properties. $C_{60}(I_h)$ has a closed electronic shell with a completely filled five-fold degenerate HOMO. Vibrational dynamics of the neutral cage fluctuate around this high symmetry structure [1]. Upon reduction and partial filling of the triply degenerate LUMO with one excess electron, the resulting open-shell cluster monoanion is thought to undergo Jahn–Teller (JT) distortion and structural rearrangement to minimize its potential energy. Possible reduced symmetries are D_{5d}, D_{2h} or D_{3d}, depending on the coupling and their relative strengths. As pseudorotation barriers in C_{60} are on the order of only a few kJ/mol, [2,3], *i.e.* similar to uncertainties of theoretical calculations, it is currently unclear which structure is populated and whether this JT effect is of static or dynamic nature.

The favourable electron-accepting capability of C_{60} is directly related to its electronic structure. As first shown by cyclic voltammetry [4,5] C_{60} can be stepwise electrochemically reduced in certain solvents up to C_{60}^{6-}. Chemical reduction is accomplished *e.g.* by reactions with alkali metals or organic agents including numerous organometallic compounds (for an overview see Ref. [6]). Solvated C_{60} and the various negatively charged fullerenes (fullerides) can also be distinguished from each other by electronic absorption spectroscopy. Different negative states have characteristic absorption bands throughout the visible and near-infrared (NIR) spectral regions [7–9].

Fullerenes have also been covalently functionalized with organic chromophores to yield dyads and triads with interesting photo- and redox-active properties – often involving negatively charged fullerene intermediates [10]. Efficient charge carrier generation in such covalently linked dyads or triads opens a new approach to transport and collection of photogenerated charges *e.g.* at electrodes [11]. Such devices require an ultrafast forward electron transfer ($\sim$ 45 fs) [12] and significantly slower recombination, typically on the millisecond timescale, thus enabling an effective charge generation [13]. Here, C_{60}^- can play an important role as intermediate resulting in longer lasting (ns) charged separated states.

Excited-state dynamics of isolated C_{60}^- have been studied using time-resolved photoelectron spectroscopy (in a molecular beam after excitation at 775 nm) [14]. The lifetime of the first electronically excited state was determined to be 2.2 ps with internal conversion as dominating relaxation channel. This finding was confirmed in solution (acetonitrile) [15], with somewhat slower electronic relaxation occurring within 3.5 ps upon excitation at 925 nm. In both studies, the underlying experimental setups did not allow real time observation of any associated JT distortion phenomena, as have been predicted for C_{60}^- in some detail [16]. The motion corresponding to JT distortion (pseudorotation), can be rationalized as connecting adiabatic potential energy surfaces in which each minimum corresponds to a specific distortion [16]. Compared to the electronic excitation energies, barrier heights between these JT minima are quite small. This together with expected ultrafast timescales (further complicated by solvent and electron donor interactions) has so far precluded direct observation.

In the present study, we significantly extend the dynamical measurements on solvated C_{60}^- by performing transient absorption and transient anisotropy measurements

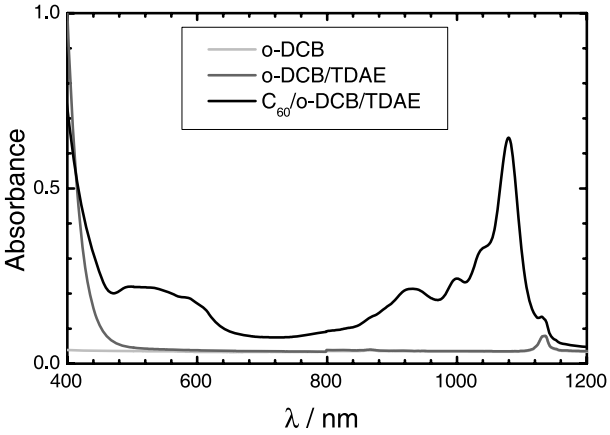

Fig. 1. Optical absorption spectrum of C_{60} in TDAE and o-DCB including the respective reference spectra (pure o-DCB and o-DCB/TDAE). The maximum around 1070 nm indicates formation of C_{60}^-, subsequent smaller peaks shifted towards smaller wavelengths are vibrational progression of the same electronic state. Around 530 nm, the second excited states of C_{60}^- can be observed.

in two different solvents. Specifically, both the first and second excited state were transiently prepared while probe wavelengths were tuned throughout the NIR region (where the first excited state absorbs and fluorescence bands are located). All results were analyzed using a simple response function applying biexponential fitting routines to all pump-probe wavelength pairs. Transient anisotropy experiments were performed after excitation to the first excited state – also including two additional vibronic transitions. As we will show below, ultrafast transient anisotropy measurements can potentially provide information on JT distortions observable in real-time.

2. Experimental section

2.1 Preparation of C_{60}^-

C_{60}^- in solution can be chemically prepared by various experimental techniques [7,17–19]. Here we employed two kinds of electron donors added to the respective fullerene solutions: tetrakis(dimethylamino)ethylene (TDAE) and elemental sodium.

(a) Solutions of C_{60}^- in o-dichlorobenzene (o-DCB; Merck Chemicals, purity $> 99\%$) were prepared by adding tetrakis(dimethylamino)ethylene (TDAE; TCI Chemicals) to a solution of C_{60} (Alfa Aesar, purity $> 99.5\%$) in o-DCB according to the procedure described in Ref. [20]. In the present study, we used a 100 fold excess of TDAE with respect to the molarity of C_{60} to ensure a suitable optical density (OD) of typically 0.1–1 at the desired pump wavelengths. Using extinction coefficients reported in the literature [6] this corresponds to a concentration range from 5×10^{-5} to 5×10^{-4} mol/l. Fig. 1 represents a steady-state absorption spectrum of C_{60}^- in o-DCB together with reference measurements. The formation of C_{60}^- is indicated by a pronounced absorption band peaking at 1070 nm with shoulders shifted to lower wavelengths attributable to vibronic progression [17,21–23]. An additional broad ab-

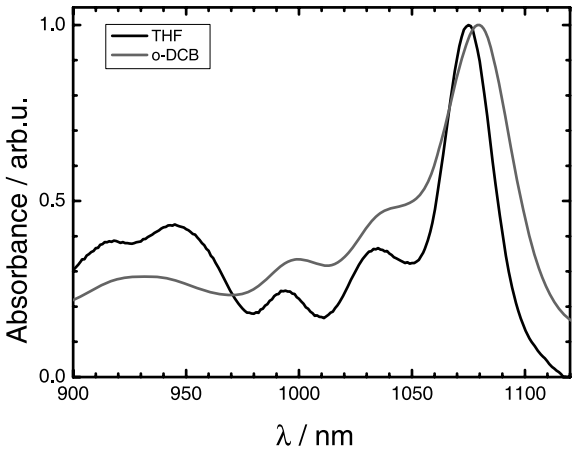

Fig. 2. Comparison of the optical absorption spectra of the first electronic transition in THF (black) and o-DCB (grey), enlarged version of the one shown in Fig. 1a at room temperature (optical path length: 1 mm).

sorption feature appears at wavelengths between 500 and 650 nm corresponding to the second optically allowed excited state.

(b) Solutions of C_{60}^{-} in tetrahydrofuran (THF) were prepared using elemental sodium. In general, care has to be taken so as not to "overshoot" the correct concentration of added sodium metal because the tendency to form C_{60}^{2-} dianions is much stronger in Na/THF solutions than in TDAE/o-DCB. Also, it is of utmost importance to perform all steps in the absence of air. Before use, THF (Fluka, 99.5%) was dried over sodium and a small amount of benzophenone as indicator for water traces. In another stock flask, C_{60} and sodium (Merck, 99%) were introduced. It turned out to be necessary to purify sodium by heating it under vacuum conditions with a heat gun. This was accomplished by placing a small piece of sodium into the mixing chamber, slightly above C_{60} to avoid direct contact. After heating, dried THF was added by vacuum condensation. Upon allowing the THF(s)/Na(s)/C_{60}(s) mixture to warm to room temperature, C_{60}^{-} formed within two days as determined by UV-Vis/NIR absorption spectroscopy using a Varian/Cary 5E spectrometer. Spectra of C_{60}^{-} in o-DCB and THF are compared in Fig. 2. Apart from small solvatochromic shifts of about 5 nm, the general band shape including vibrational progression features at 1000 and 1038 nm is comparable. Below 950 nm, the formation of C_{60}^{2-} is observable in THF but not in o-DCB. Therefore, the transients measured in THF at shorter wavelengths can represent a superposition of two different charge states of reduced C_{60}.

In both C_{60}^{-} solutions prepared according to methods a) and b) additional bands around 530 nm were observed due to direct excitations of the second excited state.

2.2 Setup of the femtosecond experiment

Time-resolved pump-probe absorption spectroscopy and transient anisotropy measurements were carried out in order to investigate the ultrafast photophysics of solutions contained in 0.25 ml quartz cuvettes (Hellma, QS) having an optical pathlength of

1 mm. Pump and probe laser pulses were derived from two separate noncollinear optical parametric amplifiers (NOPAs) tunable from 470 to 1600 nm which were pumped by a commercial 1 kHz amplified femtosecond Ti:sapphire laser system (Clark-MXR, CPA 2210). The pulse duration of the NOPA pulses was about 80 fs depending on the wavelength. The pump pulse was temporally delayed relative to the probe pulses using a computer controlled translation stage (Melles Griot; Physik Instrumente for delays longer than 150 ps) and mechanically chopped at 500 Hz.

Transient anisotropy was recorded by simultaneously detecting the parallel and perpendicular component of the probe beams. For this, the polarization of the probe beam was set to 45° using a tunable half-wave plate (Alphalas). The transient anisotropy $r(t)$ was then obtained from the relation

$$r(t) = \frac{\Delta OD_{\parallel}(t) - \Delta OD_{\perp}(t)}{\Delta OD_{\parallel}(t) + 2 \cdot \Delta OD_{\perp}(t)} . \quad (1)$$

In all experiments, the pump pulse energy (at various wavelengths) was about 0.6–0.8 μJ, while the probe pulse energy was less than 10 nJ. The probe beam diameter at the experiment was less than half of the pump beam, which was about 2 mm. Both laser beams were weakly focussed into the sample to compensate for the divergence of the NOPA pulses. All data were processed by an analog-to-digital converter (NI-PCI6034E), which was controlled by a programme written in LabView (National Instruments).

3. Results

3.1 Excitation at 1070 nm in o-DCB

Figure 3 represents transients at a pump wavelength of 1070 nm and various probe wavelengths studied for solutions of C_{60}^- in o-DCB at room temperature. Depending on the probe wavelength, complex transient responses were found. At degenerate pump and probe wavelengths, an ultrafast transient bleach of C_{60}^- is observed which is readily assigned to ground state depopulation and subsequent recovery on a timescale of tens of ps. At probe wavelengths beyond 1070 nm, two different features were observed. First, between 1100 and 1200 nm, the initial bleach is followed by an induced absorption which itself decays on a tens of ps timescale. At 1300 nm, we observed pump-induced bleach only, with a similar decay time as for the fast component at 1070 nm. However, in contrast to the situation at 1070 nm for which the bleach represents ground state depopulation, this cannot be the case at 1300 nm because there is no significant ground state absorption at this wavelength. Instead, given that this region corresponds to the red part of the C_{60}^- fluorescence band, we assign the transient to stimulated emission from the first excited state. Blue-shifting the probe to 1000 nm results in a transient bleach with a time constant, τ_1, comparable to degenerate probing at 1070 nm. In this case, a second time constant, τ_2, is not necessary to fit the data appropriately.

All transients in Fig. 3 were fit by a biexponential fitting routine convoluted with a Gaussian line-shape in order to mimic the cross correlation of the pump and probe overlap and to account for group velocity dispersion due to the 1 mm sample thickness (solid lines). Typically (with the exception of 1000 and 1300 nm probes), the relaxation

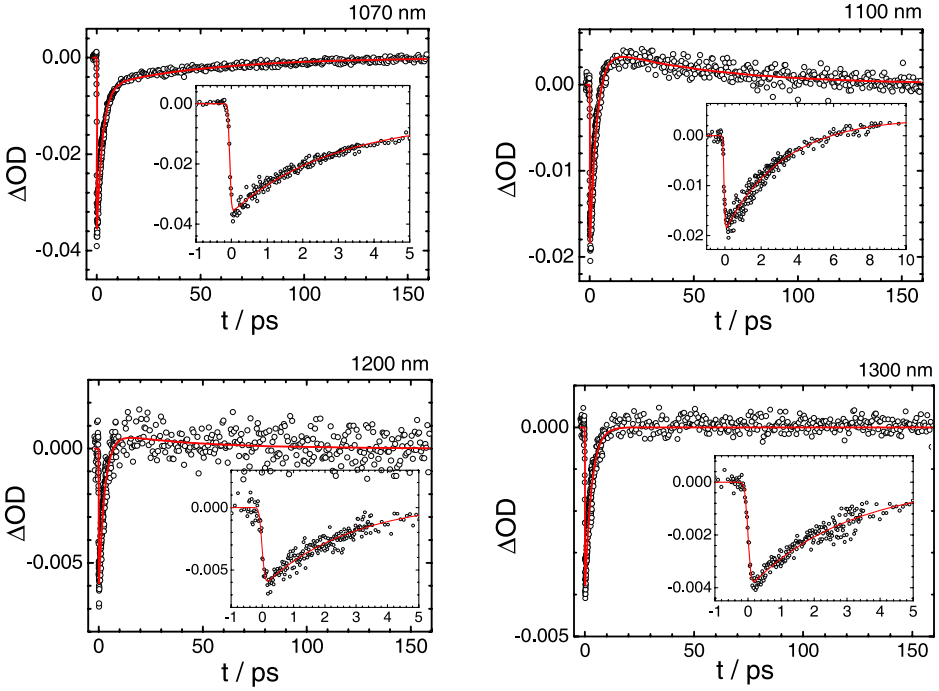

Fig. 3. Transient response of C_{60}^- in o-DCB after excitation at 1070 nm (probe wavelengths as indicated). The insets highlight the early-time dynamics. Solid line: biexponential fit convoluted with instrument function.

dynamics were well described by two different time constants. These were on the order of 3 and 70 ps, respectively (see Table 1 for details). While the first time constant indeed represents a constant within an overall variance of $\sim 10\%$, the second time constant fluctuates between 40 and 70 ps, depending strongly on the probe wavelengths.

3.2 Excitation at 1000 and 950 nm in o-DCB

Figure 4 displays transients at a pump wavelength of 950 nm and probe wavelengths as indicated. Qualitatively, the transients agree with those at a pump wavelength of 1070 nm. For the degenerate case, but also at slightly red-shifted wavelengths up to 1070 nm, only ultrafast bleach is found. However, at a probe wavelength of 1100 nm, the bleach is followed by an induced absorption, as was the case at the same probe wavelength after 1070 nm excitation. At longer wavelengths (1300 nm, not shown) stimulated emission dominates the transient as was the case after 1070 nm excitation. Fits to the corresponding transients (see Table 1), show that pumping at 1070, 1000 or 950 nm leads to near quantitatively the same relaxation dynamics. Therefore, the structured shape of the stationary absorption spectrum peaking roughly at 1070, 1000 and 950 nm can be assigned to the same electronic state – in agreement with previous gas phase results [24].

Table 1. Fitting parameters (equation see below) for the transient response at room temperature of C_{60}^- in o-DCB solution at various pump-probe wavelength combinations (pulse duration $\Delta\tau_p = 70$ fs for 1070–950 nm excitations and 150 fs for 530 nm excitation depended on probe wavelengths and group velocity mismatch between pump and probe beams)

$$\Delta\mathrm{OD}(t) = \left[1 + \mathrm{erf}\left(\frac{\sqrt{4\ln(2)}\cdot t}{\Delta\tau_p}\right)\right] \cdot \sum_{i=1}^{2} A(\text{or } B)\cdot \exp\left(-\frac{t}{\tau_i}\right) \tag{2}$$

and

$$w(A)/\% = \frac{|A|}{|A|+|B|}. \tag{3}$$

λ(pump-probe)/nm	τ_1/ps	A	$w(A)$/%	τ_2/ps	B
1070/1000	2.99	−0.004			
1070/1070	2.81	−0.0153	83	52.1	−0.0031
1070/1100	3.26	−0.0119	84	68.3	0.0023
1070/1125	3.26	−0.00137	85	66.3	0.00025
1070/1150	2.81	−0.00345	83	52.4	0.0007
1070/1200	2.91	−0.00355	91	40.3	0.00037
1070/1300	3.04	−0.002			
1000/1070	2.93	−0.00048		72.0	−0.00012
1000/1125	3.29	−0.00011			
1000/1150	2.79	−0.00033	83	58.2	0.00007
950/950	2.88	−0.0037			
950/1000	2.78	−0.00365			
950/1100	3.23	−0.0165	85	74.9	0.0030
950/1150	2.44	−0.0049	86	51.2	0.0008
950/1200	2.57	−0.0031	91	44.6	0.0003
950/1300	1.73	−0.00122			
532/950	2.21	−0.00125			
Fast component: 89 fs					
532/1000	2.18	−0.00127			
Fast component < 50 fs					
530/1070	2.06	−0.00089	78	77.9	−0.00025
530/1200	1.84	−0.00066	82	54.2	0.00015
530/1250	1.91	−0.00044	73	57.8	0.00006
532/1300	1.61	−0.00048			
Fast component: 111 fs					

3.3 Excitation at 530 nm in o-DCB

Excitation at 530 nm leads to an immediate bleach at 1070 nm, the peak of the resonance of the first excited state (see Fig. 5). Pump-limited bleaching is also observed at probe wavelengths of 1000 and 950 nm corresponding to different vibronic transitions of the same electronic excitation. Beyond 1100 nm, an induced absorption follows bleaching, as was the case after photoexcitation of the first excited state. Analyzing the amplitude ratio for the first and second components of the time-dependent response (see

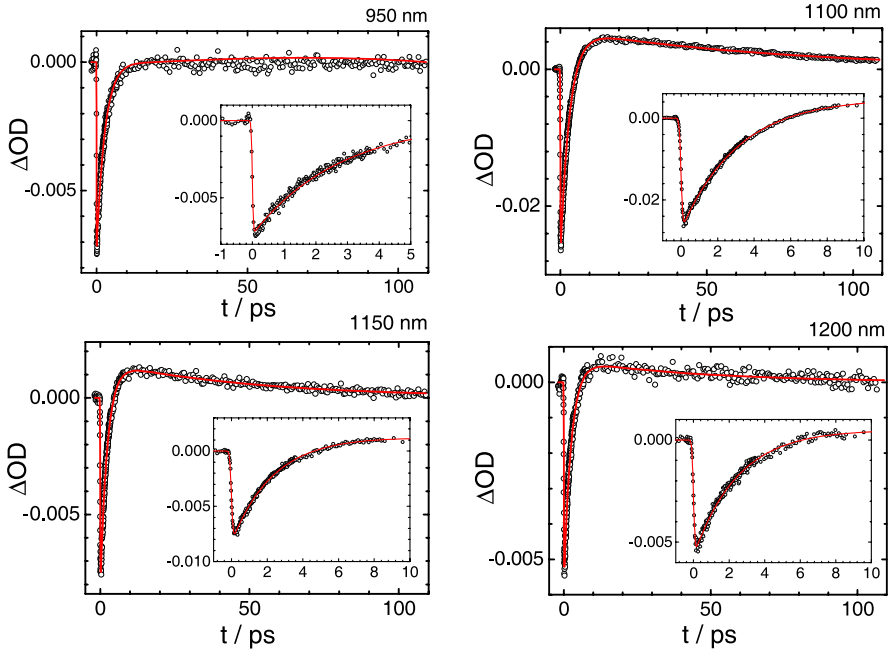

Fig. 4. Same as in Fig. 3 but with 950 nm excitation.

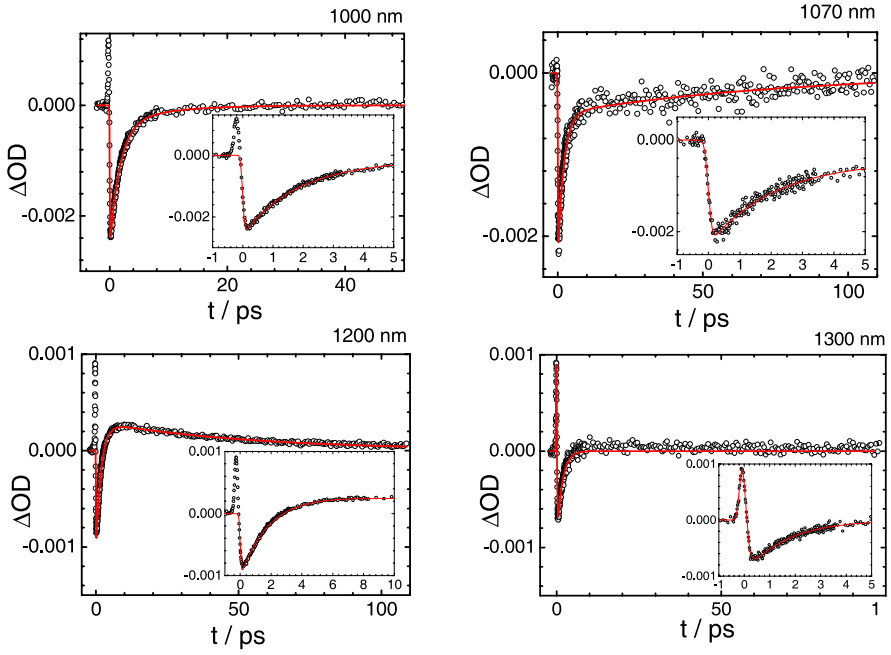

Fig. 5. Same as in Fig. 3 but with 530 nm excitation.

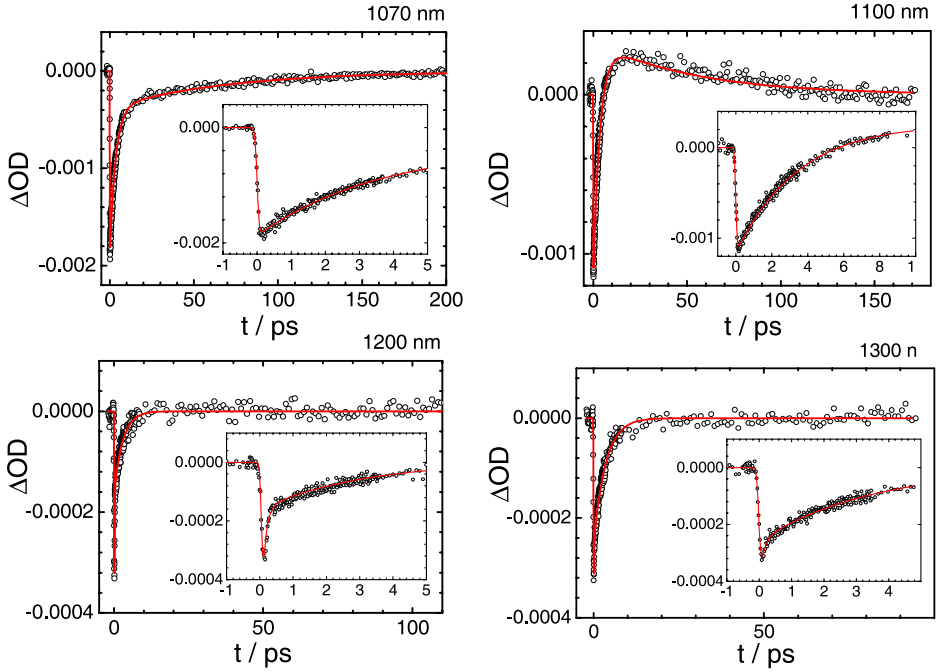

Fig. 6. Transient response of C_{60}^- in THF after excitation at 1070 nm and probe wavelengths as indicated. The insets highlight the early-time dynamics. Solid line: biexponential fit convoluted with instrument function.

Table 1) reveals that induced absorption at 1200 nm is more pronounced after excitation of the second excited state than was seen upon directly populating the first excited state. At 1300 nm, bleach dominates the transient with a recovery time, which was found to be almost twice as fast as that observed after pumping the first excited state. It is also worth noting that most transients show a sharp immediate rise before bleaching sets in. Usually, one would attribute such behaviour to cross correlation artefacts of the sample (especially due to the solvent and/ or the quartz windows). However, it may also indicate pump-induced absorption of the first excited state. If so, the timescale for transition from the second to the first excited state would be much faster than 150 fs and as such masked by the limited time resolution of our experimental setup. This is primarily given by the group velocity mismatch between pump and probe laser pulses. Such a fast rate for internal conversion would indicate a strong coupling mechanism between both states, *e.g.* conical intersection.

3.4 Excitation at 1070 nm in THF

The corresponding pump-probe transients of C_{60}^- in THF are shown in Fig. 6. The time constants were determined analogously to the procedure for o-DCB solutions. Qualitatively, the transients are similar to those obtained in o-DCB, *i.e.*, bleach at 1070 nm, bleach and absorption between 1100 and 1200 nm and finally, bleach again at 1300 nm.

Table 2. Fitting parameters for the transient response at room temperature of C_{60}^- in THF at various pump-probe wavelength combinations. The faster time constants for τ_1 in the last three lines are a consequence of the superposition of mono- and dianion dynamics. See Table 1 for information on the parameters.

λ(pump-probe)/nm	τ_1/ps	A	$w(A)$/%	τ_2/ps	B
1070/1070	3.48	−0.00075	80	69.5	−0.00019
1070/1100	3.60	−0.00075	81.3	53.0	0.00017
1070/1200	2.89	−0.00008			
Fast component: 103 fs					
1070/1300	3.45	−0.00013			
Fast component: 121 fs					
950/950	0.73	−0.00947	81	41.4	−0.00223
950/1000	0.57	−0.00426	77	44.1	0.00121
840/950	0.74	−0.00253	76	48.3	−0.00078

Quantitatively, the time constants τ_1 are about 15% larger than for o-DCB – a significant increase outside of the experimental error range. Table 2 lists all time constants obtained at various pump-probe wavelength combinations in THF solvent.

3.5 Excitation at 950 nm in THF

Care has to be taken when C_{60}^- is excited at 950 nm in THF (see Table 2). Often, we found much faster time constants 1 as compared to measurements in o-DCB. This behaviour is in line with the optical absorption spectrum of the fulleride in THF, where the optical density increases below 950 nm, indicating the onset of formation of C_{60}^{2-}. Contrarily, there are no signs of such a process in o-DCB. In reasonable agreement with a recent publication [15], we observe an ultrafast relaxation time constant of 0.6–0.7 ps. In addition, we can identify a longer component on a tens of ps timescale that is similar to the one in o-DCB and also similar to our observation after 1070 nm excitation in THF (see Table 2). At 950/1000 nm the initial bleach turns into an induced absorption, which was not the case in o-DCB. Again, this is direct consequence of C_{60}^{2-} formation in THF.

3.6 Transient anisotropy

Figures 7–9 represent transient absorption measurements for selected pump/probe wavelength combinations (in o-DCB). Qualitatively, the transients behave similarly independent of the wavelengths probed. For 1070/1070 nm (Fig. 7) the anisotropy $r(t)$ starts at ~ 0.15 and decreases to almost zero within 100–150 fs, *i.e.*, considerably faster than the time constant, τ_1, in the pump-probe transients. Equivalent behaviour is seen at the other pump-probe wavelength combinations. Slight differences are due to the overall amplitude at 950/950 nm (Fig. 9) which is 0.5 mOD and therefore near the experimentally accessible limit of 50–100 μOD. Consequently, the signal-to-noise ratio is lower compared to the 1070/1070 nm measurement. Marginal residuals (< 0.01) on a ps timescale are primarily due to the detection limit of the setup and most likely do

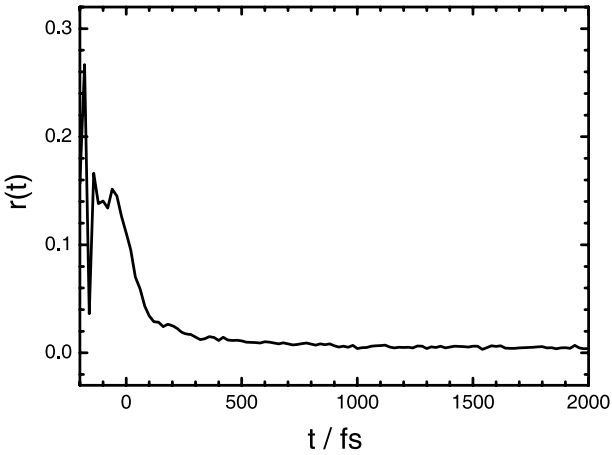

Fig. 7. Raw data of the transient anisotropy of C_{60}^- in o-DCB at a pump/probe wavelength combination of 1070/1070 nm. Around time zero, additional cross correlation artefacts are visible.

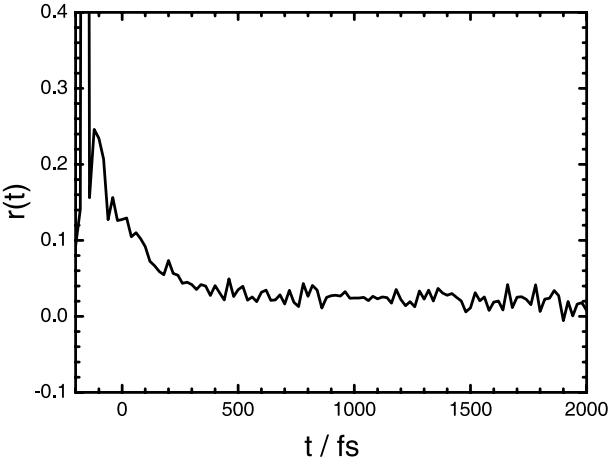

Fig. 8. Same as in Fig. 7 but with a pump/probe combination of 950/1070 nm.

not have any physical meaning. According to our analysis, the initial anisotropy, $r(0)$, is in the range of 0.15–0.2, corresponding to an angle of the transition dipole moments of 35–30°. Transient anisotropy usually monitors the time-dependent change of the transition dipole moments with respect to the initial polarization conditions. In the case of an electronic excitation, an initial value, $r(0)$, of 0.4 (corresponding to an angle of 0°) would indicate a parallel orientation of the relevant transition dipole moments between ground and excited states. In addition, $r(0)$ may depend on the signal-to-noise ratio, the uncertainty in determining time zero (about 10–20 fs) as well as the overall temporal resolution of the experimental setup. Finally, the transient anisotropy traces shown in Figs. 7–9 are convoluted with the pump-probe cross correlation contribution in the sol-

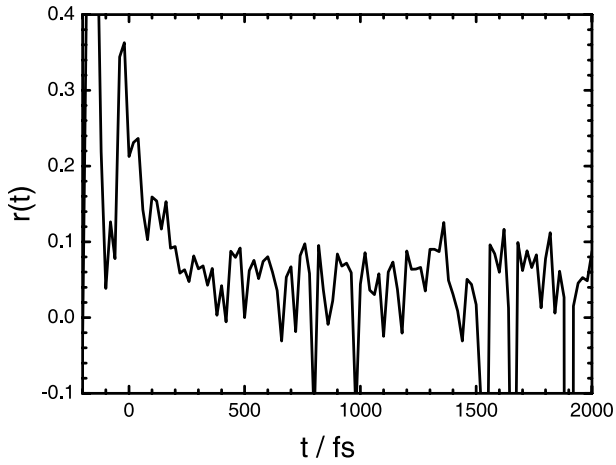

Fig. 9. Same as in Fig. 7 but with a pump/probe combination of 950/950 nm.

vent or the quartz windows of the sample cell that was not corrected for. Therefore, the absolute values of $r(0)$ determined in this study are subject to these errors.

4. Discussion

Up to now, there is no consistent picture of the ground state symmetry of C_{60}^- anion – neither in solution nor in the gas phase. For example, Echt and coworkers [24] postulated D_{5d} symmetry, while our recent ab initio calculations [14] assumed D_{3d} symmetry. Even in the solid state, the crystallographic data available do not allow clear determination of the molecular symmetry [6], although a distortion can be seen if compared to the neutral C_{60} molecule. Here again, two different symmetries are possible – D_{3d} (which is also found for the C_{60}^{2-}- dianion) or D_{5d}. Quantum chemical calculations tend to favour the D_{5d} geometry, but the D_{3d} isomer has nearly the same energy [6].

We interpreted the observed ultrafast dynamics in C_{60}^- in terms of a simple three-state level scheme (ground state and two excited states), which follows the energy scheme obtained by TDDFT calculations that were restricted to D_{3d} symmetry [14]. In this configuration the doublet ground state, $^2A_{2u}$, and and the next higher lying ^2E_u state are separated by 0.15 eV (with an uncertainty of 100 meV). These states are vibrationally interconvertible by a dynamic JT distortion. The first excited state that is reached after 1070, 1000 or 950 nm excitation would then correspond to a ^2E_g state.

4.1 Lifetime of the first excited state

From our analysis (Tables 1 and 2), we can deduce a lifetime for the ^2E_g state of ~ 3 ps in o-DCB. This value is subject to an uncertainty of $< \pm 10\%$ due to the interplay between different processes leading to ultrafast bleach and absorption contributions. To be more specific, ground state excitation at 1070 nm leads to bleaching when probed

at 1070 nm. Upon slightly shifting the probe wavelength to 1100 nm, we observe that this bleach is followed by induced absorption. Therefore, it is likely that at 1070 nm such a contribution may also exist. Although it does not dominate the overall amplitude, it may very well influence the analysis. On the other hand, if one compares the lifetimes, τ_1, measured in o-DCB and THF, a tendency towards slightly larger values in THF is apparent (increasing by about 15% to roughly 3.5 ps). Both values for τ_1 are supported by the bleach recovery observed at 1300 nm where stimulated emission prevails. Therefore, we can conclude that the lifetime of the first excited state is influenced by the local environment of C_{60}^-. While in o-DCB, TDAE is used as electron donor, sodium fulfils the same purpose in THF solution. Consequently, the local C_{60}^- environment is significantly different in these two solvents, resulting not only in the observed shift of the stationary peak position, but also in the lifetime differences.

It has been argued [14,15] that relaxation occurs predominantly by internal conversion from the first excited state to the electronic ground state. Our results for the solvents o-DCB and THF support this observation. On the other hand, we also find that stimulated emission can play a measurable role during relaxation in solution under pump-probe conditions. Independent of the solvent, we always find bleaching for probe wavelengths above 1150 nm. This cannot be interpreted as ground state depopulation because C_{60}^- fluorescence dominates in this spectral region [3]. Therefore, we attribute the ultrafast response for $\lambda > 1150$ nm to stimulated emission having the same decay time as the ground state recovery at 1070 nm. Nevertheless, in the absence of a probe pulse, internal conversion is the dominating decay channel.

Upon lowering the excitation wavelength from 1070 to 1000 and finally to 950 nm, there is a tendency towards a reduced time constant, τ_1. At 950/1300 nm, this time constant is almost a factor of 2 smaller than at 1070/1300 nm. Qualitatively, this can be understood in terms of the higher excess energy deposited into the C_{60}^- excited state. At a higher total energy, there is a correspondingly higher density of vibrational states both in the electronically excited state and in the electronic ground state – in line with the interpretation given in Ref. [25] for C_{60} energy redistribution after high-intense laser excitation. This phenomenon also explains our observation upon population of the second optically allowed excited state at 530 nm. Here, we observe a decay time constant, $\tau_1 < 2$ ps. This can be interpreted in terms of a two step decay. First an ultrafast (< 100 fs – limited presumably by the time resolution of our setup) internal conversion occurs from the second to the first excited state. Subsequent internal conversion to the ground state proceeds from the correspondingly populated highly vibrationally excited levels of the first electronically excited state. This finding is also consistent with our previous gas phase experiments [14]. Here, excitation at 775 nm was probed, *i.e.*, in the blue-wing of the first electronically excited state transition band. Note, that this experiment measured the excited state lifetime of a fully isolated moiety, *i.e.* a system in which dissipation of excess vibrational excitation to surrounding (solvent) molecules cannot occur.

Hence, we conclude that preparation of the first excited state into higher vibrational levels leads to faster internal conversion. Observation of a pulse-limited bleach at 1300 nm shows that stimulated emission occurs at this wavelength even after 530 nm excitation. This in turn suggests that relaxation from high to low vibrational levels of the first electronically excited state competes with internal conversion (as was the case after

direct excitation to the first excited state). Furthermore, there exists effective coupling of C_{60}^- to the local environment (solvent molecules as well as with TDAE and Na).

We note in closing, that for C_{60}^{2-} pumped at 950 nm in THF we observe a time constant, τ_1, of 0.6–0.7 ps – a value which is comparable to a recent study in solution (0.4 ps in Ref. [15]).

4.2 Solvent dependence and vibrational relaxation

According to high-resolution ESR spectra, C_{60}^-/TDAE solutions in toluene do not contain isolated ions, but contact pairs instead [26]. These should strongly influence energy dissipation by intermolecular vibrational relaxation. Accordingly, the time constant, τ_2, reflecting vibrational energy dissipation after internal conversion to the ground electronic state should alter upon changing the solution environment (from C_{60}^- in o-DCB/TDAE to C_{60}^- generated using Na/THF). A crosscheck is not possible, because sodium is not compatible with o-DCB, and THF is too polar to solubilise TDAE. As already pointed out, both the solvent and the electron donor influence the first excited state lifetime, τ_1, by roughly 15%. Also the second time constant, τ_2, is influenced – but in a more complex way. Inspection of the o-DCB data in Table 1 reveals that after 1070 nm excitation and probing between 1100 and 1200 nm the time constant, τ_2, decreases as expected for a vibrational relaxation process. For excitations at 1000 and 950 nm a second time constant is not necessary to adequately fit the transients for probe wavelengths below 1070 nm. Together, these observations imply a transient spectrum which appears red-shifted with respect to the (room temperature) equilibrated spectrum. This is a typical behaviour for (ground state) vibrational relaxation of an initially vibrationally "hot" ensemble generated after internal conversion. Assuming that the excitation energy of the laser pulse is equipartitioned into all C_{60}^- vibrations after internal conversion (~ 3 ps) one can estimate the internal energy U(T) using statistical thermodynamics by

$$U(T) = \sum_{i=1}^{N} \frac{R \cdot \Theta_i}{\exp\left(\Theta_i / T\right) - 1} \tag{4}$$

where N denotes the number of vibrational frequencies as calculated by DFT methods and Θ_i are the corresponding vibrational temperatures. For example, an excitation at 1070 nm would correspond to a temperature rise from 300 to roughly 405 K (within the harmonic approximation) resulting in a smooth red-shift of the absorption spectrum. This is observed as a pump-induced absorption on a ps timescale as seen in Figs. 3–5 for a probe wavelength of 1100 nm. Tuning the probe wavelength to 1200 nm results in a significant reduction of the pump-induced absorption; thus providing further support for our assignment of vibrational relaxation in the electronic ground state (for a more detailed discussion of the dependence of vibrational relaxation on probe wavelengths in a different chromophore system see *e.g.*, Ref. [27]). Also, considerable changes in time constants as a function of probe wavelengths – in our case from 40 to 70 ps – are indications of vibrational relaxation. To exclude alternative interpretations such as multiphoton excitation and excited state absorption, we also performed intensity-dependent

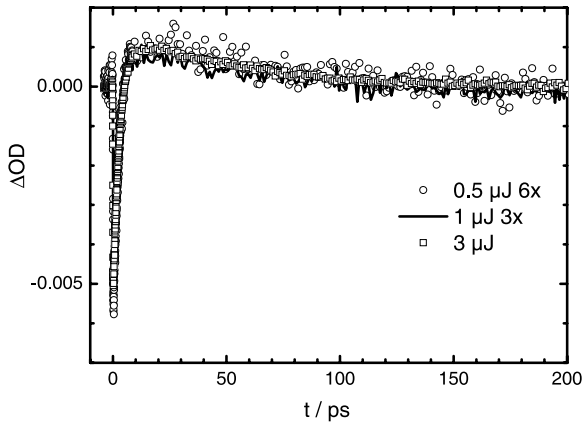

Fig. 10. Intensity dependent measurement of C_{60}^- in o-DCB at a pump/probe wavelength combination of 1070/1150 nm. Excitation energies as indicated. The transient response for 0.5 μJ is multiplied by 6, that for 1 μJ by 3 to better demonstrate the linearity of the amplitudes on a ps timescale.

measurements at a probe wavelength of 1150 nm (see Fig. 10). As can be seen, the amplitude varies linearly with the excitation energy indicating a one-photon process under our experimental conditions.

Finally, we address the possibility of excited state absorption instead of vibrational relaxation in the electronic ground state. In principle, one could imagine that the sum of pump and probe pulses reach higher excited states, which – according to selection rules ([1 + 1] excitation) – would be a dark state with respect to one-photon ground state excitation. Such a summation is only possible within the lifetime of the excited state, which is on the order of 3 ps. However, the induced absorption in the transients appears at significantly later delay times (> 4 ps). Therefore, such a process is as unlikely as multiphoton absorption. Also, the excitation at 530 nm results in a pump-induced bleach at 1200 nm after a similar delay as observed for 1070 nm excitation, but with a stronger induced absorption. In contrast, the absorption after 1070 nm pumping is only marginal at 1200 nm. Again, this supports vibrational relaxation because the higher energy deposited into C_{60}^- leads to a higher internal energy resulting in a corresponding temperature of $\sim$ 550 K (cp. to 405 K after 1070 nm excitation). Higher internal energy is often equivalent to a stronger spectral red-shift. Finally, the timescale of 40–70 ps itself is a strong indication of vibrational relaxation. Such a value is comparable to the value of 40 ps reported for C_{60} [28,29]. In contrast to the latter, C_{60}^- allows to study vibrational relaxation in real-time without the disturbance of singlet-triplet crossing. For THF and o-DCB, we ultimately did not find a strong solvent dependence of ground state vibrational relaxation. Small differences can be rationalized in terms of slightly varying local environments [28].

4.3 Transient anisotropy

The transient anisotropy decays considerably faster than the excited state population. As transient anisotropy spectroscopy is directly sensitive to the temporal evolution

of the transition dipole moment, *i.e.*, the pump-induced change of photo-selected molecules, one can monitor both orientational changes due to intra- or intermolecular processes. Molecular rotations usually occur on timescales from hundreds of fs up to ps and cannot be the origin of the observed fast decay. Also, anisotropy decay due to collisions with solvent molecules occurs on such (longer) timescales. Consequently, we have to postulate fast motions on the excited state surface as being responsible for this ultrafast decay. Such motions may correspond either to high frequency vibrational modes of C_{60}^- or to other processes like *e.g.*, pseudorotations. The latter can be understood to first order as the rotation of a distortion – in our case a JT distortion – due to the instantaneous coupling between electronic motions and nuclear vibrations. Depending on the nature of the potential energy surfaces involved, tunnelling between different JT energy minima is possible. According to the theoretical investigations by Dunn *et al.* [16] tunnelling is of no relevance for C_{60}^- and pseudorotation is thought to be the dominant contribution here.

To our knowledge, there has so far been no direct experimental evidence for such pseudorotations under room temperature conditions. Correlation times for the freezout of JT distortions have recently been measured by NMR experiments. For example, in a 20 K measurement of the ferromagnetic phase of $TDAE^+/C_{60}^-$ a correlation time on the order of 100 ns has been found [3,30]. From theoretical considerations, Dunn *et al.* [16] postulated that the time constant for pseudorotation should be 10 fs or less. Our anisotropy decay at various wavelengths may therefore be interpreted as due to pseudorotation (or at least part of it) in the first excited state – limited by the time resolution of our setup. As a corollary, it is not clear whether the transition dipole moments of the ground and first excited states are really as different as suggested by our results (up to 35°) or whether this is due to the insufficient time resolution. In any case, transient anisotropy spectroscopy is a promising experimental tool for following pseudorotations in real-time; whether or not it will be suitable for detailed symmetry description of C_{60}^- embedded in a noncentrosymmetrical environment also comprising counterions will be subject to future investigations.

5. Conclusions

We have carried out detailed experimental studies of the excited state dynamics of C_{60}^- in two solvents, o-DCB and THF (in the presence of the electron donors TDAE and Na, respectively) by applying femtosecond pump-probe absorption and transient anisotropy spectroscopy. The transient response of C_{60}^- shows the following phenomena: (i) transient bleaching due to depopulation of the ground state of C_{60}^- at probe wavelengths between 950 and 1070 nm, (ii) transient bleaching and pump-induced absorption due to vibrational relaxation in addition to ground state depopulation between 1070 and 1150 nm and finally (iii) transient bleaching due to stimulated emission from the first electronic excited state above 1150 nm. The lifetime of the first excited state is slightly influenced by the solvent, but the excitation wavelength seems to have a stronger impact as suggested by our results after 530 nm excitation and the results from previous time-resolved photoelectron spectroscopy of isolated C_{60}^-. We obtain a first excited state lifetime of 3 ps at 1070 nm excitation decreasing to 2 ps or slightly less upon 530 nm

pumping (and ultrafast relaxation from the second to the first excited state). Excitation at 1070 nm of C_{60}^- in THF yields transients, which are essentially consistent with those observed for C_{60}^- in TDAE/o-DCB. However, C_{60}^- in THF solutions were found to be subject to considerable C_{60}^{2-} impurity formation. Anisotropy data revealed an ultrafast decay within 100 fs, *i.e.* faster than the temporal resolution of our experimental setup and corresponding to ultrafast processes occurring on the excited state potential energy surface. Vibrational motions or pseudorotation are likely reasons. In the latter case this would be the first direct experimental indication by time-resolved methods of a pseudorotation in C_{60}^- at room temperature.

Acknowledgement

This work was funded by the State Baden-Württemberg, the Karlsruhe Institute of Technology (KIT) and the Deutsche Forschungsgemeinschaft as administered through the Center for Functional Nanostructures (CFN, project C3.02). We are deeply grateful to Prof. Dr. Dr. Horst Hippler who was one of the principal investigators when the CFN was founded in 2001.

References

1. J. L. Dunn, Phys. Rev. B **69** (2004) 064303.
2. J. Cioslowski, *Electronic Structure Calculations on Fullerenes and their Derivatives*, Oxford, University Press, New York, 1995.
3. T. Kato, T. Kodama, and T. Shida, Chem. Phys. Lett. **205** (1993) 405.
4. Q. Xie, E. Perez-Cordero, and L. Echegoyen, J. Am. Chem. Soc. **114** (1992) 3978.
5. Y. Ohsawa and T. Saji, J. Chem. Soc. Chem. Commun. (1992) 781.
6. C. A. Reed and R. D. Bolskar, Chem. Rev. **100** (2000) 1075.
7. M. Baumgarten, A. Gügel, and L. Gherghel, Adv. Mater. **5** (1993) 458.
8. D. R. Lawson, D. L. Feldheim, C. A. Foss, P. K. Dorhout, C. M. Elliott, C. R. Martin, and B. Parkinson, J. Electrochem. Soc. **139** (1992) L68.
9. W. K. Fullagar, I. R. Gentle, G. A. Heath, and J. W. White, J. Chem. Soc. Chem. Commun. **6** (1993) 525.
10. A. S. D. Sandanayaka, Y. Araki, O. Ito, G. R. Deviprasad, P. M. Smith, L. M. Rogers, M. E. Zandler, and F. D'Souza, Chem. Phys. **325** (2006) 452.
11. A. M. Ramos, S. C. J. Meskers, P. A. van Hal, J. Knol, J. C. Hummelen, and R. A. J. Janssen, J. Phys. Chem. A **107** (2003) 9269.
12. C. J. Brabec, G. Zerza, G. Cerullo, S. De Silvestri, S. Luzzati, J. C. Hummelen, and S. Sariciftci, Chem. Phys. Lett. **340** (2001) 232.
13. I. Montanari, A. F. Nogueira, J. Nelson, J. R. Durrant, C. Winder, M. A. Loi, N. S. Sariciftci, and C. Brabec, Appl. Phys. Lett. **81** (2002) 3001.
14. O. T. Ehrler, J. P. Yang, C. Hättig, A. N. Unterreiner, H. Hippler, and M. M. Kappes, J. Chem. Phys. **125**(2006) 074312.
15. M. J. Hope, M. P. Higlett, D. L. Andrews, S. R. Meech, I. D. Hands, J. L. Dunn, and C. A. Bates, Chem. Phys. Lett. **474** (2009) 112.
16. J. L. Dunn, I. D. Hands, and C. A. Bates, J. Mol. Struct. **838** (2007) 60.
17. M. A. Greaney and S. M. Gorun, J. Phys. Chem. **95** (1991) 7142.
18. H. Moriyama, H. Kobayashi, A. Kobayashi, and T. Watanabe, Chem. Phys. Lett. **238** (1995) 116 and references therein.
19. J. Stinchcombe, A. Penicaud, P. Bhyrappa, P. D. W. Boyd, and C. A. Reed, J. Am. Chem. Soc. **115** (1993) 5212.

20. P.-M. Allemand, K. C. Khemani, A. Koch, F. Wudl, K. Holczer, S. Donovan, G. Gruner, and J. D. Thompson, Science **253** (1991) 301.
21. T. Kato, T. Kodama, T. Shida, T. Nakagawa, Y. Matsui, S. Suzuki, H. Shiromaru, K. Yamauchi, and Y. Achiba, Chem. Phys. Lett. **180** (1991) 446.
22. T. Kato, T. Kodama, M. Oyama, S. Okazaki, T. Shida, T. Nakagawa, Y. Matsui, S. Suzuki, H. Shiromaru, K. Yamauchi, and Y. Achiba, Chem. Phys. Lett. **186** (1991) 35.
23. G. A. Heath, J. E. McGrady, and R. L. Martin, J. Chem. Soc. Chem. Commun. (1992) 1272.
24. S. Tomita, J. U. Andersen, E. Bonderup, P. Hvelplund, B. Liu, S. B. Nielsen, U. V. Pedersen, J. Rangama, K. Hansen, and O. Echt, Phys. Rev. Lett. **94** (2005) 053002.
25. I. Shchatsinin, T. Laarmann, N. Zhavoronkov, C. P. Schulz, and I. V. Hertel, J. Chem. Phys. **129** (2008) 204308.
26. M. Fujitsuka, C. Luo, and O. Ito, J. Phys. Chem. B **103** (1999) 445.
27. O. Schalk, H. Brands, T. S. Balaban, and A. N. Unterreiner, J. Phys. Chem. A **112** (2008) 1719.
28. S. Shenogin, P. Keblinski, D. Bedrov, and G. D. Smith, J. Chem. Phys. **124** (2006) 014702.
29. (a) H. Kim, D. Bedrov, G. D. Smith, S. Shenogin, and P. Keblinski, Phys. Rev. B **72** (2005) 085454; (b) S. T. Huxtable, D. G. Cahill, S. Shenogin, and P. Keblinski, Chem. Phys. Lett. **407** (2005) 129.
30. P. Jeglič, R. Blinc, T. Apih, A. Omerzu, and D. Arcon, Phys. Rev. B **68** (2003) 184422.